Journal of Applied Physics

Drop deposition affected by electrowetting in direct ink writing process

Cite as: J. Appl. Phys. **126**, 035302 (2019); https://doi.org/10.1063/1.5109385
Submitted: 08 May 2019 . Accepted: 18 June 2019 . Published Online: 17 July 2019

J.-M. Löwe, J. Plog, Y. Jiang, Y. Pan, and A. L. Yarin

Journal of Applied Physics ARTICLE scitation.org/journal/jap

Drop deposition affected by electrowetting in direct ink writing process

Cite as: J. Appl. Phys. **126**, 035302 (2019); doi: 10.1063/1.5109385
Submitted: 8 May 2019 · Accepted: 18 June 2019 ·
Published Online: 17 July 2019

View Online Export Citation CrossMark

J.-M. Löwe,[1,2,a)] J. Plog,[1,a)] Y. Jiang,[1] Y. Pan,[1,b)] and A. L. Yarin[1,b)]

AFFILIATIONS

[1]Department of Mechanical and Industrial Engineering, University of Illinois at Chicago, 842 W. Taylor St., Chicago, Illinois 60607-7022, USA
[2]High-Voltage Laboratories, Technische Universität Darmstadt, Fraunhoferstr. 4, 64283 Darmstadt, Germany

[a)]**Contributions:** J.-M. Löwe and J. Plog contributed equally to this work.
[b)]**Authors to whom correspondence should be addressed:** yayuepan@uic.edu and ayarin@uic.edu

ABSTRACT

Direct ink writing (DIW) is a three-dimensional printing process that fabricates objects by depositing a functional ink on a substrate in a layer-by-layer way, for a wide range of applications including flexible electronics, scaffolds, biostructures, and so on. In DIW, adhesion between inks of different materials, and between the ink and the substrate, remains to be a challenge. In the context of the DIW process, the present work aims at determining the influence of the electric field on the adhesion of several commonly used and commercially available inks to different materials including glass, Kapton tape, ceramics, and other hydrophobic surfaces. The electric field is applied after or during different stages of the printing process, and the results are compared to reference specimens. The blister test is employed to measure the adhesion energy, which characterizes the bond between different materials. The main goal is to determine the enhancement of adhesion between different materials by means of the electric field and thus the improvement of the quality of printed items.

I. INTRODUCTION

Direct ink writing (DIW) is a class of additive manufacturing (AM) techniques which deposit functional and/or structural liquid materials onto a substrate in digitally defined locations.[1,2] Based on the dispensing form, DIW could be classified as droplet-based (e.g., piezoelectric ink jetting) or filament-based. DIW differs from the conventional AM in terms of the following characteristics: (i) the range of materials deposited can include metals,[3] ceramics[4] and polymers,[5,6] electronically and optically functional materials,[7,8] as well as biological materials including living cells;[9,10] (ii) the track width ranges from submicrometers to millimeters; and (iii) the substrate is an integral part of the final product.[1,2] A wide variety of applications from flexible electronic fabrication to functional tissue printing has been demonstrated during the past 20 years.

However, despite all this progress, grand challenges in the ink-substrate interaction still exist and thus cause various manufacturing defects. For example, many DIW manufacturing defects, including coffee-ring effect, bulging, liquid puddles, liquid splashing, scalloped, or discontinuous line, are caused by the undesired wetting and spreading of liquid on the substrate. Furthermore, for full functionality, multiple inks with varied chemical compositions and properties need to be printed on different substrates, which sometimes are superhydrophobic. In such multimaterial direct ink writing processes, inks should be compatible with the substrate and form a proper bond with previously deposited materials or the substrate.[1,2] Insufficient cohesion between layers of inks or adhesion between the ink and the substrate will cause large interface resistance or even material separation failures. All these challenges majorly stem from the ink-substrate interaction, especially the wettability of the substrate by the ink.[11–14]

All efforts that have been made to adjust the ink-substrate interaction are focused on substrate surface modification,[15–17] including changing substrate chemical composition by coating a new layer or changing the surface topology. Yet, the chemical modification sometimes is not desirable as it affects the functionality and properties of the final product. The surface topology modification methods, including plasma treatment and surface machining, are time-consuming, costly, and the modified surface may easily get damaged during the DIW process. Lastly and most importantly, all

those surface modification methods cannot dynamically and locally adjust the wettability, are irreversible, and cannot control the wettability of both the substrate and the deposited layers in a layer-by-layer direct writing process. Lack of these capabilities significantly limits the choice of inks and the direct writing performance.

In this work, we investigate electrowetting for dynamic and local control of the ink-substrate wetting properties and hence the adhesion strengths. Moreover, we provide a direct method of measurement of the adhesion energy. In the past, several attempts to use the electric field to influence and optimize the printing process were reported.[18] In most cases, the electric field is applied between the needle and the specimen similarly to electrospinning.[19] Accordingly, in such cases as in Zhang *et al.*,[18] the control of drop behavior using the electric field is very limited. In this work, we introduce a novel electrowetting setup, in which the electric field is applied on the printing surface and can be programed in a pixel-by-pixel fashion using coded electrodes.

Several inks, including photosensitive inks as well as silicone-based inks which are beneficial for production of flexible electronics, have been characterized in this work. Deposition of these inks on various substrates, including glasses, wood, Kapton tape, superhydrophobic coating surface, and ceramic surface, has been investigated. Overall, in direct ink writing, the range of inks deposited can include metals, ceramics, and polymers, functional composites as well as biological materials. In addition, the substrate which could be flat, curvilinear, round, flexible, irregular or inflatable, is usually an integral part of the final product. Due to the large material difference of the ink and the substrate, as well as the varied topology of the substrate, the ink-substrate adhesion can be very weak, leading to manufacturing challenges or even defects, such as separation of the printed layer from the substrate or undesirable moving of the ink on the substrate before the full solidification, and so on. Experiments were performed to analyze the effect of the electric field on the deposition of these inks. Blister tests were conducted to characterize the influence of electrowetting on the interfacial adhesion of printed samples. The rest of this paper is organized as follows. Section II describes the experimental setup, methods, materials, and process. Experimental results are presented in Sec. III. The adhesion energy of samples printed under different electric field settings is measured and discussed. Finally, conclusions are drawn in Sec. IV.

II. MATERIALS AND METHODS

A. Blister test

To measure the adhesion energy between the dried printed ink and the supporting material, blister tests are employed. Such tests have already been used in the past to measure the adhesion and cohesion energy between polymers, nanofiber mats, and substrates and other thin films.[19–25] The blister test characterizes adhesion of two materials, which is determined by the shape of the blister and the force causing it.[23,25] Delamination of the dried printed ink from the substrate caused by the pushing shaft results in the formation of a blister, i.e., a new free surface is exposed, which requires work conducted by the shaft. The exact blister shape in the case of soft stretchable blister materials (in distinction from the stiff blister materials) was found theoretically in Ref. 23 (also, cf., Ref. 25) as a solution of the membrane equation.[26] In particular, the axisymmetric blister geometry depicted in Fig. 1 is found as

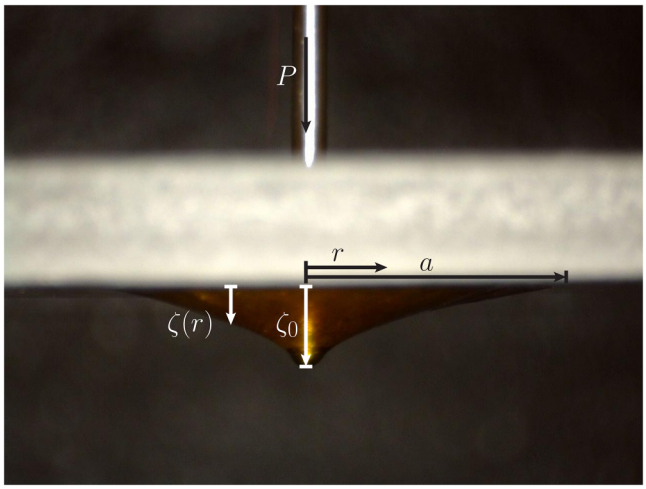

FIG. 1. Blister configuration photographed in the experiment with the parameters of Eq. (1) superimposed.

$$\zeta = \frac{3}{2}\left(\frac{Pa^2}{\pi Eh}\right)^{1/3}\left[1-\left(\frac{r}{a}\right)^{2/3}\right], \tag{1}$$

where P is the force applied by the shaft which results in blister formation, a is the base radius of the blister, E is Young's modulus of the dried printed layer, h is the thickness of this layer, and r is the radial coordinate centered at the shaft and belonging to the base plane of the blister.

Accordingly, the maximum blister height is

$$\zeta_0 = \frac{3}{2}\left(\frac{P}{\pi Eh}\right)^{1/3} a^{2/3}. \tag{2}$$

It should be emphasized that the force P and the blister radius a are directly measured in the blister test. Then, the adhesion energy T is calculated as follows:[21,23]

$$T = \frac{3}{8}\left(\frac{1}{\pi^4 Eh}\right)^{1/3}\left(\frac{P}{a}\right)^{4/3}. \tag{3}$$

The adhesion energy is measured in J/m^2.

Note that in the fracture mechanics, the energy G, which is needed to create a new surface, is associated with the rate of release of the elastic energy U per unit area A and an imposed displacement δ: $G = (\delta U/\delta A)_\delta$. For a plane stress or strain and fracture in mode I indicated by the index, the energy G is given by

$$G_{\mathrm{I}} = \frac{K_{\mathrm{I}}^2}{E'} = \frac{K_{\mathrm{I}}^2(1-\nu^2)}{E}, \tag{4}$$

where K_{I} is the stress intensity factor for mode I and ν is Poisson's ratio; $E' = E/(1-\nu^2)$. The value of G_{I} is associated with the

surface energy γ of the two banks of the newly created crack,

$$G_I = 2\gamma, \tag{5}$$

i.e., $G_I = T$.

In the experiments, the ink is printed on a specimen support, which is placed upside down on the stage of the mechanical testing machine (Instron 5942). Further explanation of the setup along with a schematic can be found in Sec. II B, and a photograph of the actual setup used can be found in the supplementary material (Fig. S1). A blister is formed using an Instron 5942 with a 500 N load cell. A shaft with a diameter of 0.8 mm is used to form the blister and delaminate the printed ink from the support medium. The shaft is attached to the load cell, which generates the blister using an advancing rate of 10 mm/min. This rate was used to ensure that the blister is formed practically instantaneously. The shaft enters a through hole in the specimen support and only touches the solidified ink. The blister formation is captured underneath by a digital USB microscope (Dino-light edge) with 20–220× magnification capable of taking 5 MP pictures at a frame rate of 10 fps. At the start of the experiment, the video data as well as the data recorded by the Instron are synchronized. Both the force and the extension of the shaft are recorded by the load cell of the Instron with an accuracy of ±0.5% of the reading and ±0.02 mm, respectively. The tests were conducted until the sample fails due to bursting of the blister or if the blister has a diameter larger than ∼20 mm, which is larger than the field of view of the digital microscope. Afterward, the video and the recorded data are analyzed using an in-house Matlab code to determine the diameter of the blister and to correlate the data with the measured load. A video of blister formation is imported into MATLAB and manually synchronized with the data of the Instron machine by using an optical indicator, which facilitates the calculation of the adhesion energy. Note that the corresponding image of the blister is shown and its diameter is ascertained by the boundary line. The sensitivity of the analysis has been estimated too. Finally, the adhesion energy is calculated using Eq. (3).

B. Specimen preparation

To measure the adhesion of the solidified inks on different substrates, several inks and substrate materials are tested. In general, the ink is printed on a surface of a substrate, which has a size of ∼25 mm × ∼75 mm, with a through hole of 1 mm diameter at the center. To test realistic material combinations, the adhesion of a commercially available photosensitive ink, as well as a silicone-based ink were explored. These are already commonly used materials in 3D printing.[1,2,5,7] Substrate materials tested in this study include commercial Kapton tape, sandblasted glass, chemically etched glass, glass coated with a commercially available hydrophobic coating (Never Wet), wood, and ceramics.

To prepare blister test specimens using the Kapton tape as a substrate material, a fiberglass board is used as the support with a central hole concentric to the one in the tape. Such a support is required to prevent bending of the tape during the blister test. The specimen preparation is done very carefully to ensure the repeatability. The fiberglass boards are cleaned with ethanol and electrodes are eventually adhered at 15 mm–25 mm from each other, depending on the desired electric field strength. Both the fiberglass board and the electrodes are subsequently covered with the Kapton tape and a hole with a diameter of 1 mm is drilled in the Kapton tape to ensure the free motion of the shaft.

To prepare specimens with sandblasted glass as the substrate, microscope slides are sandblasted for 3 s and cleaned afterward with water. A diamond drill bit is used to drill a 1 mm hole through the glass, and the specimen is then cleaned with ethanol. For the chemically etched glass specimen substrate, the procedure of sandblasting is replaced by chemical etching. A commercial etching cream (Armour Etch Cream) is applied on the glass for 1 h. Afterward, the glass is cleaned with water and the specimen is treated the same way as the sandblasted one. For the coated glass sheet substrate, clean glass without any etching or sandblasting is used. After the through hole is drilled, the surface is coated with the two-component coating (Rust-Oleum Never Wet). The coating itself is not cleaned again because it is very sensitive regarding mechanical abrasion and the surface properties might be influenced by solvents like ethanol, which would result in a low repeatability. It should be noticed that only inks (EcoFlex), which are repelled by the coating, are tested with this substrate. Similarly to the glass specimens, the diamond drill bit is used to drill a hole in the ceramic specimen, which is then cleaned with ethanol.

The hole for the shaft must be covered to prevent the ink from leaking into it during the direct writing process. Different covering methods have been tested. In the first method, wax was used to fill the hole up and clog it. After printing on the specimen, the wax was then removed by melting at its low melting temperature of ∼37 °C. However, several trials revealed that the blister testing of specimens prepared using this wax-based method has a large variability. Specifically, for the specimens produced with the electric field, it seems that the photosensitive ink still can enter the hole filled with wax and, therefore, affect the measurement results. It was recognized that the electric field forces the ink to move in the electric field and increases the surface wetting. Hence, it is possible that the ink creeps into the hole in addition to wax. To address this leaking problem, we applied an alternative covering method, that is, instead of filling with wax, the hole is covered with a small piece of the Kapton tape, which is adhered to the surface to seal the hole. The corresponding schematic is shown in Fig. 2.

C. Inks

For the preparation of silicone ink, EcoFlex 00-30 was purchased and used as received. This type of silicone solidifies at room temperature in 4 h by mixing part A and part B in a 1:1 ratio. In this study, 5 g of part A, 5 g of part B, and 0.1 g of silicone retarder (Smooth-On Slo-Jo) are mixed at 2000 rpm for 3 min (viscosity of 30 g/cm s), followed by centrifugation for 1 min (AR-100, Thinky; a planetary centrifugal mixer) before printing. Young's modulus of Ecoflex 00-30 is 27 kPa.[27]

For the preparation of photopolymer ink (viscosity of 4 g/cm s), a flexible resin (product code Spot-E, Spot-A Materials, Spain; https://spotamaterials.com/wp/wp-content/uploads/2015/07/Spot-E_MSDS_tmp.pdf) was purchased and used as received. Spot-E is nonwater based photo-polymerizable resin in the near-UV and visible spectrum, which is highly stretchable after curing. The Young's modulus of solidified Spot-E is given by the manufacturer

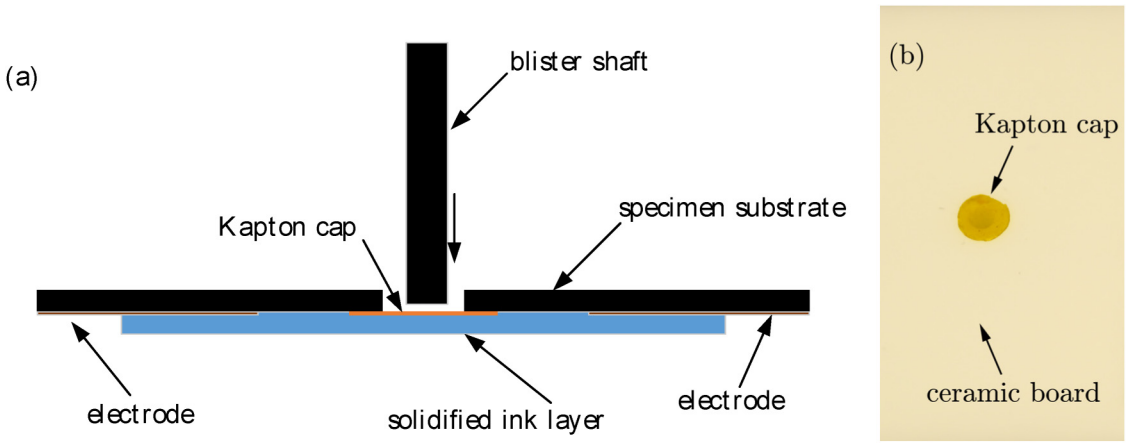

FIG. 2. (a) Principle of the blister testing setup, including the specimen substrate, Kapton cap, electrodes, and the through hole for the shaft in the blister test. (b) Image of a Kapton cap on a ceramic board ready for 3D printing.

as $E = 12$ MPa. To verify this value, several tensile tests were performed, which revealed that the Young's modulus value strongly depends on the force and the extension. The measurement results at three different extension rates are shown in Fig. 3. At very low strains, Young's modulus is $E = 12$ MPa and is independent of the extension rate as shown in the inset in Fig. 3 (indicated by the dashed circle).

The inks used in this study did not manifest any non-Newtonian effects and can be considered as viscous Newtonian liquids.

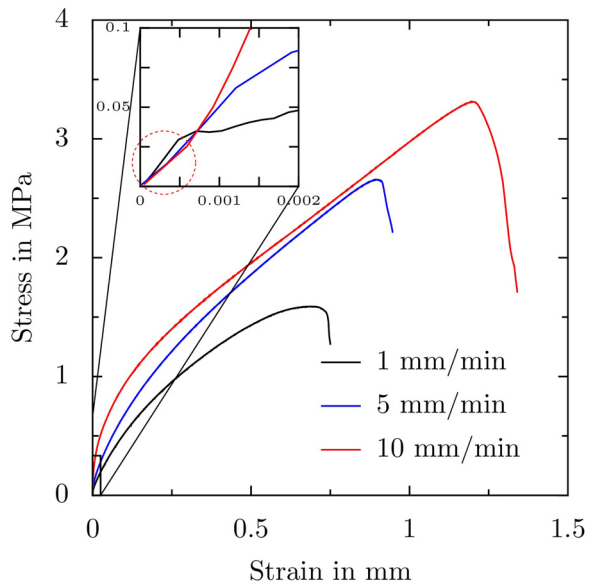

FIG. 3. Stress–strain curves for Spot-E at three different extension rates. The inset shows the small-strain range (encompassed by the dashed circle) where the Young's modulus of 12 MPa was measured.

D. Printing process

The system used for direct ink writing (DIW) experiments was developed by modifying a dispensing robot (E3V, Nordson EFD) and a schematic is shown in Fig. 4. The experiments were conducted by extruding inks through dispensing tips onto a moving platform in a trace-by-trace and layer-by-layer way. The air pressure and the vacuum level were accurately controlled by dispensers (Ultimus I and Ultimus III, Nordson EFD). Traces were directly written using various stationary blunt stainless-steel syringe tips with inner diameters in the 0.10 mm–0.41 mm range and a pump system coupled with a motorized X-Y stage. The ink was prepared by loading the solutions in a 10 cm^3 syringe barrel. The experimental setup also contains a pressure controller, which can regulate the ink flow rate. The syringe tip was fixed to a Z stage. The standoff distance was adjusted according to the tip gauge in each experiment. The DIW setup is connected to the external electronics to fully functionalize a controllable electric field. A home-made high-voltage power source is used to generate the electric field. A multimeter is utilized to monitor the real-time potential across the two copper electrodes placed 25 mm apart from each other. The electric field strength is between 200 V/mm and 400 V/mm.

To initiate printing, the stage was reset to the origin point. Upon reaching the starting position of a trace, the preprogramed ink flow began immediately after the start of the platform motion at the rate regulated by the applied pressure.

The printing pattern for fabricating the blister test specimens was a 20 mm × 20 mm square pattern. To print this square pattern, a back-and-forth path with a trace gap ranging from 0.5 mm to 1.0 mm was programed.

Printing settings for fabricating blister test specimens using Ecoflex were as follows. A dispensing tip of 0.96 mm inner diameter (18 gauge) is placed above the substrate at an approximately 0.50 mm standoff distance (because Ecoflex possesses a significant viscosity). The air pressure is set at 3 psi, and the substrate speed is set at 10 mm/s. A 1.0 mm printing trace gap is used.

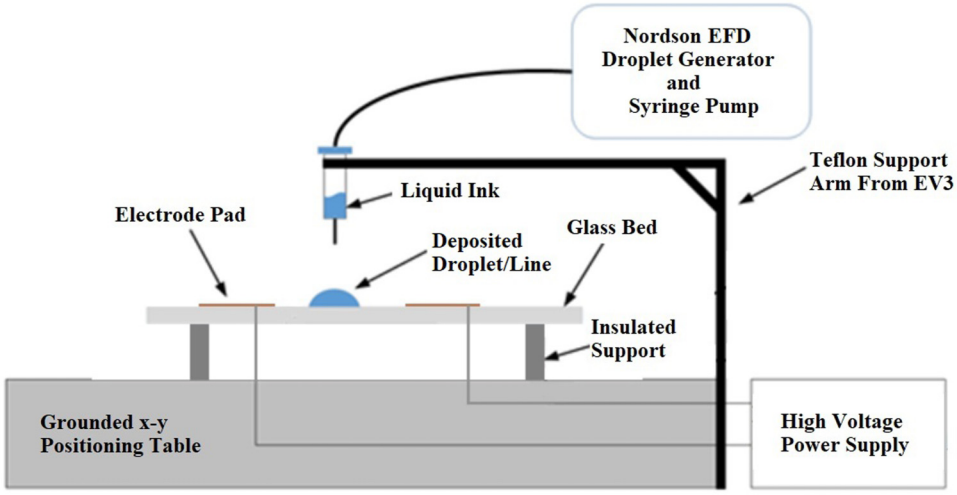

FIG. 4. Sketch of the printing setup using a modified Nordson printer with the electrode location shown.

Printing settings for fabricating blister test specimens using Spot-E were as follows. A dispensing tip of 0.43 mm inner diameter (23 gauge) is placed above the substrate at an approximately 0.20 mm standoff distance. The air pressure is set at 3 psi, and the substrate speed is set at 5 mm/s. A 0.5 mm printing trace gap is used.

III. RESULTS AND DISCUSSION

A. Blister formation and force-displacement curves

It is of interest to study the influence of the electric field on the adhesion energy of the material deposited under different manufacturing conditions. In this study, tests were performed with an electric field applied at different phases during the manufacturing process: (i) immediately after the ink has been printed onto a substrate, and (ii) during printing and the subsequent curing process. The curing of Spot-E ink can be subdivided into two stages: the precuring stage, which is ~2 min directly during printing (only applicable if UV-light is used) and the postcuring of all specimens together, which lasts ~45 min to ensure complete solidification of the ink Spot-E. Specifically for Spot-E, a third manufacturing process (iii) is defined by applying the electric field during printing and using UV light to cure the ink while printing. The Ecoflex samples are dried at ambient temperature or in the oven at a temperature of 65 °C. It should be emphasized that in some cases, precuring during printing was not used, as specified in Secs. III B–III D.

The blister test is performed for all specimens in the same way to ensure comparison between the individual samples. Because a circled piece of the Kapton tape was used to cover the through hole in the substrate by adhering to the printing surface, it influences the force-extension curve as well as the blister formation. Figure 5 shows a typical force-extension dependence of the tested specimens.

In the beginning of the experiment, the shaft has to form a blister and to delaminate the Kapton tape. The force increases steeply because the Kapton tape strongly adheres to the surface. This corresponds to region I in Fig. 5, where the diameter of the blister is practically equal to the size of the cap. As soon as the Kapton cap has been delaminated from the surface, the force diminishes, whereas the blister precursor increases in diameter (region II in Fig. 5). The force-extension curve is almost linear in region II. The data analysis is performed using this linear part of the curve, because Ref. 23 showed that the same value of the adhesion energy is found using any point on the linear slope. Accordingly, the extension of 2.5 mm was chosen as a characteristic point for the analysis of the blister diameter where the force responsible for blister formation is measured with an extension rate of 10 mm/min. As soon as a blister rips or its size reaches the size of the printed layer, the measured force abruptly diminished and the experiment was stopped. Figure 6 shows three snapshots from one of the videos, which illustrate the blister border detection by Matlab in the specimens made of sandblasted glass, etched glass substrates, and ceramic substrate. The blister radius a at the moment of its formation (the extension of 2.5 mm) is determined from such images. The load P at the moment of blister formation is measured using the load-extension curve similar to the one in Fig. 6.

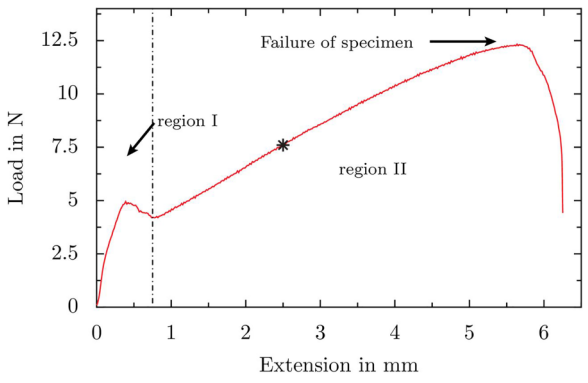

FIG. 5. Typical load–extension curve measured in the blister test of Spot-E. Region I corresponds to the delamination of the Kapton tape, and region II corresponds to the blister formation. The extension of 2.5 mm marked by an asterisk is used in data processing.

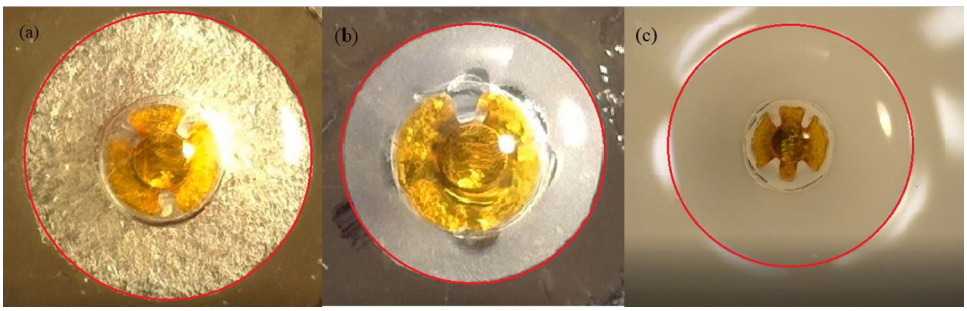

FIG. 6. Blister formation of Spot-E on (a) sandblasted glass, (b) chemically etched glass, and (c) ceramics. In all cases, the shaft extension is 2.5 mm. The blister borders are highlighted by red circles.

The Young's modulus E of the solidified coating is found in tensile tests conducted using the Instron 5942 independently.

It should be emphasized that the blister formation is different for the several tested inks due to the different ink properties. After the initial blister formation, the blister diameter increases continuously in the case of Spot-E; in contrast, the Ecoflex ink is much more flexible so that the diameter of the blister does not increase that much after the initial formation. As a result, the blister has a more elongated shape and the measured forces are much smaller in the case of Ecoflex compared to Spot-E. Overall, at least six specimens of every material were investigated to measure their adhesion energy on different substrates.

B. Adhesion energy in the cases where electric field was applied immediately after the ink has been printed onto a substrate

Here, samples are printed on specimens without the influence of electric field and no additional irradiation is added to the surrounding light. After the printing process is finished, the electric field is applied during the postcuring stage (during drying outside of the printer). Table I and Fig. 7 list the measured adhesion energies of Spot-E on different materials.

The data reveals that in the majority of these cases, the adhesion energy is not changed due to the application of the electric field, except the case of the Kapton tape, where the adhesion energy has been lowered due to the application of the electric field. In all the other cases, the mean values of the adhesion energy are close with and without the electric field, whose standard deviation is quite large due to the large variation of the individual experiments. The curing rate of Spot-E used in these experiments is ~0.1 mm in 15 s or less, i.e., the region near the three-phase contact line is cured relatively fast and the contact line surroundings are essentially pinned to the substrate surface.

C. Adhesion energy in the cases where electric field was applied during printing and during the subsequent curing process

In contrast to Sec. III B, here the electric field is also applied during printing as well as the postcuring. In this scenario, the ink is immediately influenced by the electric field after being issued from the needle. In particular, it acts on droplets during their spreading over the substrate surface and enhances spreading. The electric field continues to be applied during the subsequent curing

TABLE I. The measured adhesion energy of Spot-E on Kapton, glass, and ceramic substrates with and without the electric field; (EF) denotes the cases where the electric field has been applied. The applied voltage was 7.5 kV.

Substrate	Number of specimens	Mean adhesion energy (J/m^2)	Standard deviation (J/m^2)
Kapton	25	89.39	19.21 (21.49%)
Kapton (EF)	20	39.41	14.48 (36.74%)
Ceramics	8	326.15	33.49 (10.27%)
Ceramics (EF)	7	327.13	76.07 (23.25%)
Glass—sandblasted	6	310.69	46.93 (15.11%)
Glass—sandblasted (EF)	5	297.80	42.69 (14.34%)
Glass—etched	6	265.90	60.46 (22.74%)
Glass—etched (EF)	4	241.20	37.93 (15.73%)

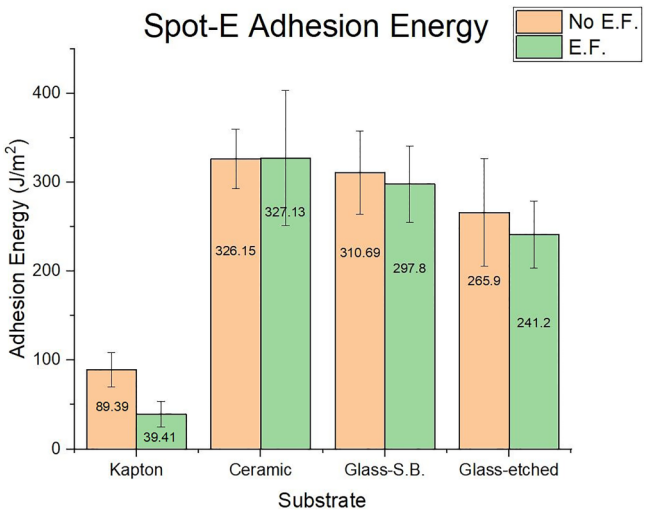

FIG. 7. The measured adhesion energy of Spot-E on Kapton, glass, and ceramic substrates with and without the electric field; (EF) denotes the cases where the electric field has been applied. The applied voltage was 7.5 kV.

TABLE II. The measured adhesion energy of Spot-E on ceramics, glass, and wood substrates with and without the electric field; (EF) denotes the cases where the electric field has been applied. The applied voltage was 7.5 kV.

Substrate	Number of specimens	Mean adhesion energy (J/m^2)	Standard deviation (J/m^2)
Ceramics	6	401.13	94.93 (23.67%)
Ceramics (EF)	17	411.12	52.48 (12.77%)
Glass—sandblasted	5	462.75	38.58 (8.34%)
Glass—sandblasted (EF)	4	512.19	8.51 (1.66%)
Glass—etched	4	480.56	51.49 (10.71%)
Glass—etched (EF)	5	507.49	112.49 (22.17%)
Wood	5	612.88	80.25 (13.09%)
Wood (EF)	5	505.61	59.37 (11.74%)

process (the postcuring) because turning it off would abruptly remove the stretching electric force and thus cause deposit shrinkage. Table II and Fig. 8 show the measured adhesion energies of Spot-E on different substrates including ceramics (purchased from Amazon), sandblasted, and etched glasses (the roughness of both types of glass is much lower than the thickness of the deposited layers), as well as wood.

The results listed in Table II and Fig. 8 show that the electric field has no major influence on the adhesion energy when applied to Spot-E during printing. For glass and ceramic substrates, the mean values of the adhesion energy are slightly higher with the electric field applied. Still, considering the standard deviation, which is quite large, the increase in the adhesion energy cannot be claimed. The large standard deviation is caused by the varying substrate properties. Even though the specimens are prepared carefully,

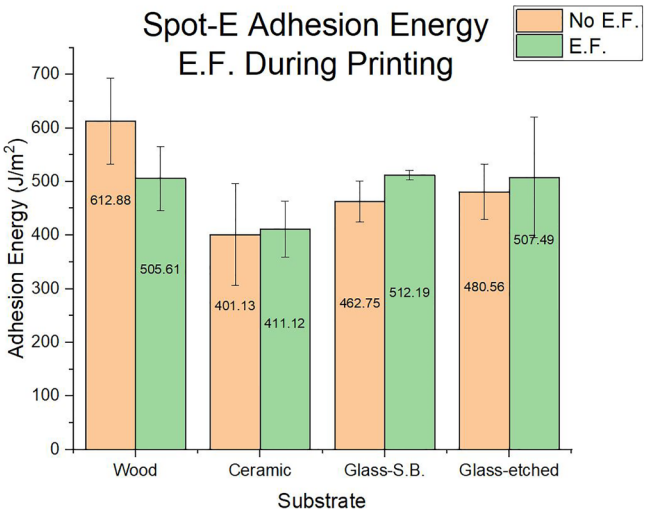

FIG. 8. The measured adhesion energy of Spot-E on ceramics, glass, and wood substrates with and without the electric field; (EF) denotes the cases where the electric field has been applied. The applied voltage was 7.5 kV.

TABLE III. The measured adhesion energy of Ecoflex 00-30 on wood, glass, and Never Wet substrates with and without the electric field; (EF) denotes the cases where the electric field has been applied. The applied voltage was 7.5 kV for glass and wood. For glass coated with Never Wet, the applied voltage was 10 kV.

Substrate	Number of specimens	Mean adhesion energy (J/m^2)	Standard deviation (J/m^2)
Never Wet—dried in ambient air	5	41.36	9.86 (23.84%)
Never Wet (EF)—dried in ambient air	5	38.61	5.93 (15.36%)
Never Wet—dried in an oven	4	20.11	2.18 (10.84%)
Never Wet (EF)—dried in an oven	4	36.11	9.36 (25.92%)
Glass	6	37.61	8.40 (22.33%)
Glass (EF)	6	36.04	7.84 (21.75%)
Wood	4	49.7	7.11 (14.31%)
Wood (EF)	3	49.65	1.90 (3.83%)

the surfaces might still have some invisible defects or properties gradients, especially in the case of sandblasted or etched surfaces. These defects can have a great influence on the adhesion energy and facilitate large standard deviation.

In addition to Spot-E, another ink was used in these experiments. Namely, the silicone-based ink called Ecoflex was printed with the electric field applied and then dried in ambient air or in an oven. If the specimens are dried in ambient air, the electric field is still applied. However, during specimen drying in an oven, the electric field was switched off right before that. Table III and Fig. 9

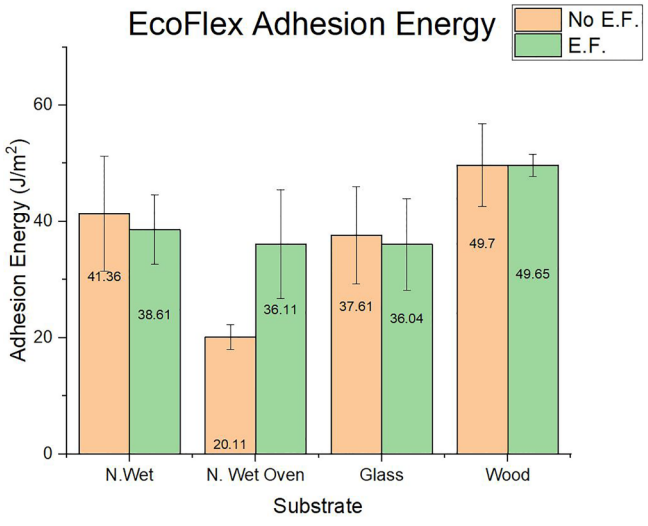

FIG. 9. The measured adhesion energy of Ecoflex 00-30 on wood, glass, and Never Wet substrates with and without the electric field; (EF) denotes the cases where the electric field has been applied. The applied voltage was 7.5 kV for glass and wood. For glass coated with Never Wet, the applied voltage was 10 kV.

list the measured adhesion energy of Ecoflex 0030 on wood (crafting plywood purchased from Menards), plane glass, and glass coated with Never Wet coating. With the latter coating, two different methods were used to dry the ink: a slow drying under ambient temperature and an accelerated drying in an oven at 65 °C.

The results in Table III and Fig. 9 reveal that there is no increase in the adhesion energy in the case of wood or plane glass substrates; the measured adhesion energies with and without the electric field are very close. In contrast, the mean adhesion energy of Ecoflex on the glass, which is coated with Never Wet is slightly higher in the case of fast drying in an oven at 65 °C. In the latter case, the standard deviation is relatively small and the increase in the adhesion is statistically sound. The hydrophobicity of the Never Wet coatings repels Ecoflex, so the ink adhesion is greatly facilitated by the electrowetting phenomenon in this case. Accordingly, the adhesion energy can be increased with an electric field if the specimens are cured very fast in an oven. This might improve the manufacturing process and increase the output due to smaller curing times, with sufficient adhesion of the printed ink to the substrate. On the other hand, the adhesion of the slowly-dried samples is unaffected by the electric field. In the case of a slow curing in ambient air, the ink has more time to adhere to the surface and, therefore, no increase due to the electric field is found.

D. Adhesion energy in the cases where the electric field is applied simultaneously with curing by UV light

The application of the electric field simultaneously with printing and curing by the UV light is only possible with the photosensitive inks. The light source is focused on the specimens during printing so that the ink is cured simultaneously while wetting the surface and affected by the electric field. Table IV and Fig. 10 list the results for all specimens formed with and without the electric field. In these cases, the specimens were directly printed onto different substrates including Kapton tape, ceramics, and sandblasted glass.

The results show that for the tested glass specimens, the mean adhesion energy is higher without the electric field compared to the specimens manufactured with the electric field applied. Nevertheless, the decrease is not statistically sound given the standard deviation. In addition, the adhesion energy on the ceramic specimens is slightly higher for the specimen subjected to the electric field compared to those without it. In the latter case, the standard deviation is rather high, 20%. Furthermore, the experiments with the Kapton tape also show that the specimens subjected to the electric field reveal a slightly higher adhesion energy than without it, even though in this case the standard deviation is higher.

TABLE IV. The measured adhesion energy of Spot-E on Kapton, glass, and ceramic substrates with and without the electric field; (EF) denotes the cases where the electric field has been applied. The applied voltage was 7.5 kV.

Substrate	Number of specimens	Mean adhesion energy (J/m^2)	Standard deviation (J/m^2)
Kapton	9	61.29	14.82 (24.18%)
Kapton (EF)	10	85.62	33.89 (39.58%)
Ceramics	9	243.15	47.11 (19.37%)
Ceramics (EF)	9	251.38	56.48 (22.47%)
Glass—sandblasted	3	346.54	67.20 (19.39%)
Glass—sandblasted (EF)	5	318.96	33.17 (10.40%)

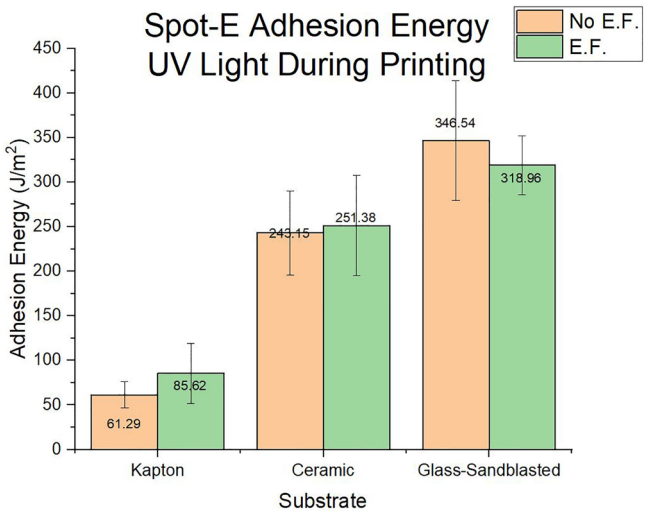

FIG. 10. The measured adhesion energy of Spot-E on Kapton, glass, and ceramic substrates with and without the electric field; (EF) denotes the cases where the electric field has been applied. The applied voltage was 7.5 kV.

E. Uncertainties

The measurement of the thickness h used in Eq. (3) for the adhesion energy is done in the middle of the specimen directly above the hole assuming the thickness of the ink layer to be constant. Specifically, for the specimens printed under the effect of the electric field, this assumption might be not very accurate and cause a rather high standard deviation. Figure 11 shows two different specimens and their surface profiles. Figure 11(a) shows a specimen formed without the electric field, and Fig. 11(b) shows a specimen, which was printed being subjected to the electric field. In both images, the red line indicates the horizontal line tangent to the surface at the highest point. In the case of Fig. 11(a), the surface of the printed ink is relatively flat and has a constant thickness. In contrast, the thickness of the ink layer has a large variation in Fig. 11(b). The highest point is in the middle of the specimen and the profile decreases on both sides, resulting in a height difference of ~0.2 mm. The fundamental theory of the blister test assumes a thin and uniform layer. Therefore, the mean adhesion energy found in the nonuniform cases can be underestimated. An increase of ~10% in the adhesion energy can be expected in such nonuniform cases.

Another factor is the uniformity of the surface. In the case of ink curing during the printing with UV light, the liquid solidification is very fast and can affect the uniformity of the surface. The printing pattern is given by the line pattern used to generate a rectangular ink layer. If a strong light source is used during the

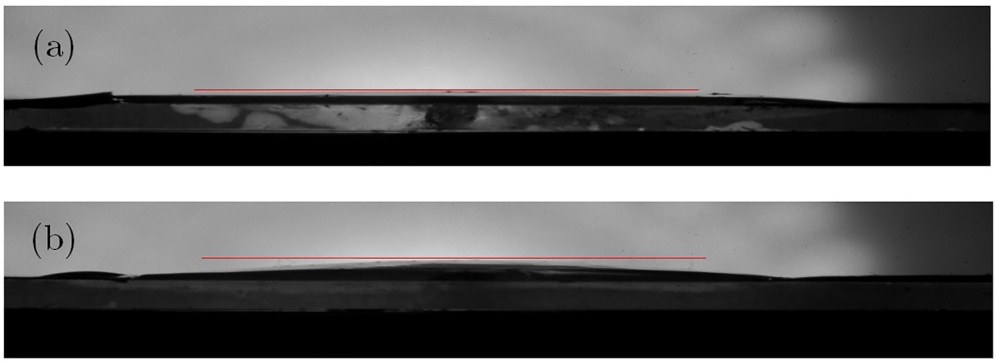

FIG. 11. Side view of a Spot-E layer printed on glass without (a) and with the electric field (b). The horizontal lines are tangents at the top of each layer. The profile is highly uniform in the case of specimens without electric field (panel a), and nonuniform for specimens printed under with the electric field (panel b). It should be emphasized that the layer thickness is an order of magnitude less than that of the substrate, and the latter can be considered absolutely rigid during the blister tests.

printing process, the ink solidifies so fast that the line pattern is still visible after printing, i.e., the lines stay apart. In the case of printing without the UV light, the ink surface has time to adjust itself due to the surface tension tending to minimize the surface area via merging the parallel printed lines and making them planar. Thus, the printing results in an almost uniform surface. Hence, the rate of curing has to be adjusted to ensure a uniform surface. Furthermore, the surface roughness is also affected by the rate of curing. A high surface roughness of the printed layer might influence the adhesion energy, as well as the uniformity of the layer properties.

IV. CONCLUSION

The experiments with different substrate materials and ink combinations revealed the effect of the electric field and the associated electrowetting on the adhesion energy. An increase in the adhesion was found for a highly hydrophobic surface (glass covered by Never Wet) in the case of a very fast curing (oven-cured) of the silicone ink. Due to the fast curing and printing, the electric field facilitates a better surface wetting and thus the resulting adhesion. Therefore, the printing process can be significantly accelerated if the electric field is applied in such cases similar to the present work. In contrast, slow curing at ambient temperature, as well as for other ink and material combinations, e.g., of Spot-E with wood, ceramics, Kapton tape, glass, or even glass with Never Wet, does not seem being affected by the electric field. Thus, the adhesion energy remains unchanged. Not even these substrates in combination (excluding Never Wet) with EcoFlex show any increase in the adhesion due to the electric field. Furthermore, the increase in the adhesion also depends on the printing process and parameters. The most promising procedure regarding EcoFlex is to use the electric field during the printing process, as well as during the postcuring stage and curing at a temperature higher than 65 °C. It should be emphasized that no precuring can be applied in this case because the material is dried by heat. Other tested methods including the application of the electric field only during the postcuring stage do not reveal a significant influence on the adhesion and only complicate the printing process. In addition, the printing process of Spot-E can be influenced by the electric field, but none of the tested methods including printing with an electric field, applying the electric field during postcuring, and using precuring with UV light during the printing process, did reveal any increase in the adhesion between the ink and the tested substrates. Since ink is not water-based, it is not repelled by the coating resulting in no increase in the adhesion.

Overall, the present experiments enhanced direct ink writing-based 3D printing capabilities on hydrophobic surfaces when silicone-based inks are used. These were achieved by the application of the electric field and the related electrowetting phenomenon and a fast curing process. Accordingly, the adhesion between the printed dried ink and the substrate was increased, and the production rate can also be increased.

SUPPLEMENTARY MATERIAL

See the supplementary material for a photograph of the actual blister setup used for experiments.

ACKNOWLEDGMENTS

This project was supported by the National Science Foundation (NSF) Grant (No. 1825626).

The authors declare no financial interests or benefits related to this research.

REFERENCES

[1]J. A. Lewis and G. M. Gratson, "Direct writing in three dimensions," Mater. Today **7**(7), 32–39 (2004).
[2]K. K. B. Hon, L. Li, and I. M. Hutchings, "Direct writing technology—Advances and developments," CIRP Ann. Manuf. Technol. **57**(2), 601–620 (2008).
[3]M. A. Skylar-Scott, S. Gunasekaran, and J. A. Lewis, "Laser-assisted direct ink writing of planar and 3D metal architectures," Proc. Natl. Acad. Sci. U.S.A. **113** (22), 6137–6142 (2016).
[4]J. A. Lewis, J. E. Smay, J. Stuecker, and J. Cesarano, "Direct ink writing of three-dimensional ceramic structures," J. Am. Ceram. Soc. **89**(12), 3599–3609 (2006).
[5]G. Pierin, C. Grotta, P. Colombo, and C. Mattevi, "Direct ink writing of micrometric SiOC ceramic structures using a preceramic polymer," J. Eur. Ceram. Soc. **36**(7), 1589–1594 (2016).

[6]V. Francis and P. K. Jain, "3D printed polymer dielectric substrates with enhanced permittivity by nanoclay inclusion," Virtual Phys. Prototyp. **12**(2), 107–115 (2017).
[7]J. A. Lewis, "Direct ink writing of 3D functional materials," Adv. Funct. Mater. **16**(17), 2193–2204 (2006).
[8]H. W. Tan, T. Tran, and C. K. Chua, "A review of printed passive electronic components through fully additive manufacturing methods," Virtual Phys. Prototyp. **11**(4), 271–288 (2016).
[9]D. J. Odde and M. J. Renn, "Laser-guided direct writing for applications in biotechnology," Trends Biotechnol. **17**(10), 385–389 (1999).
[10]D. Therriault, R. F. Shepherd, S. R. White, and J. A. Lewis, "Fugitive inks for direct-write assembly of three-dimensional microvascular networks," Adv. Mater. **17**(4), 395–399 (2005).
[11]Y. Gao, H. Li, and J. Liu, "Direct writing of flexible electronics through room temperature liquid metal ink," PLoS One **7**(9), e45485 (2012).
[12]Q. Zhang, Y. Zheng, and J. Liu, "Direct writing of electronics based on alloy and metal (DREAM) ink: A newly emerging area and its impact on energy, environment and health sciences," Front. Energy **6**(4), 311–340 (2012).
[13]J. Hu and M. F. Yu, "Meniscus-confined three-dimensional electrodeposition for direct writing of wire bonds," Science **329**(5989), 313–316 (2010).
[14]B. Derby, "Inkjet printing ceramics: From drops to solid," J. Eur. Ceram. Soc. **31**(14), 2543–2550 (2011).
[15]M. Kuang, L. Wang, and Y. Song, "Controllable printing droplets for high resolution patterns," Adv. Mater. **26**(40), 6950–6958 (2014).
[16]J. Z. Wang, Z. H. Zheng, H. W. Li, W. T. S. Huck, and H. Sirringhaus, "Dewetting of conducting polymer inkjet droplets on patterned surfaces," Nat. Mater. **3**(3), 171–176 (2004).
[17]S. Vunnam, K. Ankireddy, J. Kellar, and W. Cross, "Surface modification of indium tin oxide for direct writing of silver nanoparticulate ink micropatterns," Thin Solid Films **531**, 294–301 (2013).
[18]B. Zhang, J. He, X. Li, F. Xu, and D. Li, "Micro/nanoscale electrohydrodynamic printing: From 2D to 3D," Nanoscale **8**(34), 15376–15388 (2016).
[19]A. L. Yarin, B. Pourdeyhimi, and S. Ramakrishna, *Fundamentals and Applications of Micro- and Nanofibers* (Cambridge University Press, Cambridge, 2014).
[20]K. T. Wan and Y. W. Mai, "Fracture mechanics of a shaft-loaded blister of thin flexible membrane on rigid substrate," Int. J. Fract. **74**(2), 181–197 (1996).
[21]H. Na, P. Chen, K. T. Wan, S. C. Wong, Q. Li, and Z. Ma, "Measurement of adhesion work of electrospun polymer membrane by shaft-loaded blister test," Langmuir **28**(16), 6677–6683 (2012).
[22]M. W. Lee, S. An, H. S. Jo, S. S. Yoon, and A. L. Yarin, "Self-healing nanofiber reinforced polymer composites. 2. Delamination/debonding and adhesive and cohesive properties," ACS Appl. Mater. Interfaces **7**, 19555–19561 (2015).
[23]C. Staszel, A. L. Yarin, and B. Pourdeyhimi, "Polymer adhesion in heat-treated nonwovens," J. Appl. Polym. Sci. **135**(15), 46165 (2018).
[24]S. An, D. J. Kang, and A. L. Yarin, "A blister-like soft nano-textured thermo-pneumatic actuator as an artificial muscle," Nanoscale **10**(35), 16591–16600 (2018).
[25]A. L. Yarin, M. W. Lee, S. An, and S. S. Yoon, *Self-Healing Nanotextured Vascular Engineering Materials* (Springer Nature Switzerland AG, 2019).
[26]L. D. Landau and E. M. Lifshitz, *Theory of Elasticity* (Pergamon Press, Oxford, 1970).
[27]P. Boonvisut, and M. C. Cavusoglu, IEEE/ASME Transactions on Mechatronics **18**(5), 1602–1611 (2013).